

## OH 12.8–0.9: A New Water-Fountain Source

David A. Boboltz

*U.S. Naval Observatory,  
3450 Massachusetts Ave., NW, Washington, DC 20392-5420,  
dboboltz@usno.navy.mil*

and

Kevin B. Marvel

*American Astronomical Society,  
2000 Florida Ave., NW, Suite 400, Washington, D.C., 20009-1231,  
marvel@aas.org*

### ABSTRACT

We present observational evidence that the OH/IR star OH 12.8–0.9 is the fourth in a class of objects previously dubbed “water-fountain” sources. Using the Very Long Baseline Array, we produced the first images of the H<sub>2</sub>O maser emission associated with OH 12.8–0.9. We find that the masers are located in two compact regions with an angular separation of  $\sim 109$  mas on the sky. The axis of separation between the two maser regions is at a position angle of  $1.5^\circ$  East of North with the blue-shifted ( $-80.5$  to  $-85.5$  km s<sup>-1</sup>) masers located to the North and the red-shifted ( $-32.0$  to  $-35.5$  km s<sup>-1</sup>) masers to the South. In addition, we find that the blue- and red-shifted masers are distributed along arc-like structures  $\sim 10$ – $12$  mas across oriented roughly perpendicular to the separation axis. The morphology exhibited by the H<sub>2</sub>O masers is suggestive of an axisymmetric wind with the masers tracing bow shocks formed as the wind impacts the ambient medium. This bipolar jet-like structure is typical of the three other confirmed water-fountain sources. When combined with the previously observed spectral characteristics of OH 12.8–0.9, the observed spatio-kinematic structure of the H<sub>2</sub>O masers provides strong evidence that OH 12.8–0.9 is indeed a member of the water-fountain class.

*Subject headings:* circumstellar matter — masers — stars: AGB and post AGB — stars: mass-loss — stars: individual (OH 12.8–0.9)

## 1. INTRODUCTION

As asymptotic giant branch (AGB) stars evolve toward compact objects with surrounding planetary nebulae (PNe), mass-loss occurs in the spherically symmetric circumstellar envelopes (CSEs) with low ( $<30 \text{ km s}^{-1}$ ) expansion velocities. Despite the spherical symmetry in the progenitor objects, PNe typically exhibit morphologies, such as axisymmetric structures, that are clearly not formed through normal AGB mass-loss mechanisms (Tylenda et al. 2003).

Maser emission (SiO, H<sub>2</sub>O and OH) from AGB stars can provide insights into the structure and dynamics of the CSE. In late-type stars, the conditions for the formation of the various species of masers are typically met in a progression of zones. The SiO masers occur relatively close to the star and have velocities near the radial velocity of the star. The H<sub>2</sub>O and OH masers are found in the circumstellar wind region at progressively further distances from the star. The H<sub>2</sub>O and OH spectral profiles are often double peaked, and the velocity range covered by the OH is larger than that of the H<sub>2</sub>O.

There is a small but growing number of evolved stars which have been shown to deviate from this prototypical AGB envelope. These objects have been dubbed “water-fountain” sources due to their high-velocity H<sub>2</sub>O masers. To date there are three confirmed water-fountain sources: IRAS 16342–3814 (Sahai et al. 1999; Morris et al. 2003), IRAS 19134+2131 (Imai et al. 2004), and W43A (Imai et al. 2002). The H<sub>2</sub>O masers associated with these objects are characterized by wide velocity ranges  $\Delta v > 100 \text{ km s}^{-1}$ . Specifically, for IRAS 16342–3814, IRAS 19134+2131, and W43A,  $\Delta v$  is  $259 \text{ km s}^{-1}$ ,  $132 \text{ km s}^{-1}$  and  $180 \text{ km s}^{-1}$  respectively (Likkell et al. 1992, and references therein). These velocities are much greater than those of the typical OH/IR star in which differences between the blue- and red-shifted peaks of the OH masers are  $\sim 20\text{--}40 \text{ km s}^{-1}$  (te Lintel Hekkert et al. 1989) and roughly 75% of this range ( $15\text{--}30 \text{ km s}^{-1}$ ) for the H<sub>2</sub>O masers (Engels & Lewis 1996). In fact, for the two sources (IRAS 16342–3814 and W43A) that have detected OH masers, the H<sub>2</sub>O masers have a larger  $\Delta v$  than the corresponding OH.

In addition to the unusual spectral characteristics, the H<sub>2</sub>O masers associated with the water-fountain sources appear to exhibit unique spatial structures as revealed by radio interferometric images. In the first Very Long Baseline Interferometry (VLBI) study of the H<sub>2</sub>O masers toward W43A, Imai et al. (2002) showed that the water masers are formed in a collimated precessing jet with a true 3-dimensional space velocity of  $145 \text{ km s}^{-1}$ . Studies of IRAS 16342–3814 (Morris et al. 2003) and IRAS 19134+2131 (Imai et al. 2004) have yielded similar bipolar maser distributions albeit without the precession observed in W43A. The H<sub>2</sub>O masers toward IRAS 16342–3814 and W43A are also more extended than the OH masers in these sources. The bipolar jets traced by the H<sub>2</sub>O masers, presumably along the polar axis of the star, may represent the onset of the axisymmetric morphologies that typify PNe. The dynamical ages of the jets for IRAS 19134+2131 and W43A are estimated to be  $\sim 50 \text{ yr}$  and  $\sim 40 \text{ yr}$  respectively (Imai et al. 2002, 2004). That for IRAS 16342-3814 is estimated to be  $\sim 150 \text{ yr}$  (Claussen et al. 2004). Thus the evolutionary stage that these water-fountain sources represent is likely very short, so such objects must be quite rare.

Maser emission from OH 12.8–0.9 was first observed by Baud et al. (1979) who classified it as a Type II OH/IR star because of its characteristic double-peaked 1612-MHz OH maser profile. The star has been associated with the infrared source IRAS 18139-1816 (te Lintel Hekkert et al. 1989) which is  $\sim 26$  arcsec away. The exceptional spectral characteristics of the H<sub>2</sub>O masers toward OH 12.8–0.9, were first highlighted by Engels et al. (1986). Gómez et al. (1994) used the Very Large Array (VLA) to show that the “anomalous” H<sub>2</sub>O and OH maser emission was coincident to within 1”, and therefore belonged to the same source. Gómez et al. (1994) also found double-peaked profiles for both the OH and the H<sub>2</sub>O with the peaks of the OH separated by  $\sim 23$  km s<sup>-1</sup> and H<sub>2</sub>O peaks separated by nearly twice this amount,  $\sim 42$  km s<sup>-1</sup>. Although the velocity range for the H<sub>2</sub>O is not as wide as the other water-fountain sources, Engels (2002) found that the shape and variations in the spectra are consistent with the water-fountain class and are compatible with an axisymmetric wind. Engels suggested that OH 12.8–0.9 may represent an earlier evolutionary stage of water fountain, and that the H<sub>2</sub>O maser velocities may increase with increasing post-AGB wind speeds.

Although the spectral characteristics provide a hint that OH 12.8–0.9 is related to the water-fountain sources, to verify that it is truly a member of this class requires high-resolution VLBI imaging of the H<sub>2</sub>O maser emission. We therefore observed the H<sub>2</sub>O masers associated with OH 12.8–0.9 using the Very Long Baseline Array (VLBA) in order to map the maser distribution. In this article, we present the first VLBI images of the H<sub>2</sub>O masers toward OH 12.8–0.9 and discuss the nature of this interesting source.

## 2. OBSERVATIONS AND REDUCTION

We observed the 22.2 GHz H<sub>2</sub>O and both the 1612 MHz satellite-line and the 1667 MHz main-line OH maser emission from OH 12.8–0.9 ( $\alpha = 18^h 16^m 49^s.23, \delta = -18^\circ 15' 01''.8$ , J2000). Observations of the H<sub>2</sub>O masers occurred on 2004 June 21 for 5 hrs starting at 04:43 UT (JD 2453177.7). Observations of the OH masers occurred in two 5 hr epochs on 2004 March 16 starting at 11:04 UT (JD 2453081.0) and 2004 July 25 starting at 02:29 UT (JD 2453211.6). OH 12.8–0.9 and three continuum calibrators (1751+096, J1832–2039, and 3C 345) were observed using the 10 stations of the VLBA. The VLBA is operated by the National Radio Astronomy Observatory (NRAO).<sup>1</sup> Reference frequencies of 22.23508, 1.61223, and 1.66736 GHz were used for the H<sub>2</sub>O, the OH satellite-line, and the OH main-line maser transitions respectively. The H<sub>2</sub>O data were recorded in dual circular polarization using two 8-MHz (112.6 km s<sup>-1</sup>) bands centered on the local standard of rest (LSR) velocity of  $-58.0$  km s<sup>-1</sup>. System temperatures and point source sensitivities were on the order of  $\sim 120$  K and  $\sim 9$  Jy K<sup>-1</sup> respectively. The OH data were recorded in dual circular polarization using four 0.5-MHz (92.7 km s<sup>-1</sup>) bands centered on the LSR velocity of  $-58.0$  km s<sup>-1</sup>.

---

<sup>1</sup>The National Radio Astronomy Observatory is a facility of the National Science Foundation operated under cooperative agreement by Associated Universities, Inc.

System temperatures and point source sensitivities were on the order of  $\sim 160$  K and  $\sim 9.5$  Jy K $^{-1}$  respectively.

The data were correlated at the VLBA correlator operated by NRAO in Socorro, New Mexico. Auto and cross-correlation spectra consisting of 512 channels with channel spacings of 15.63 kHz ( $\sim 0.22$  km s $^{-1}$ ) and 0.98 kHz ( $\sim 0.18$  km s $^{-1}$ ) for the H $_2$ O and OH respectively were produced. Calibration was performed in accordance with standard VLBA spectral-line procedures using the Astronomical Image Processing System (AIPS) maintained by NRAO. The bandpass response was determined from scans on the continuum calibrators and was used to correct the target source data. A preliminary inspection of the auto-correlation (AC) spectra for the 10 antennas at this point showed that the 1667 MHz main-line OH transition was not detected toward OH 12.8–0.9. However, both the H $_2$ O and the 1612 MHz satellite line of OH were detected in the AC spectra of all antennas. The time-dependent gains of all antennas relative to a reference antenna were determined by fitting a template AC spectrum (from the reference antenna with the target source at a high elevation) to the AC spectra of each antenna. The absolute flux density scale was established by scaling these gains by the system temperature and gain of the reference antenna. Errors in the gain and pointing of the reference antenna and the atmospheric opacity contribute to the error in the absolute amplitude calibration, which is accurate to about 15–20%.

To correct any instrumental delay, a fringe fit was performed on the continuum calibrator scans and residual group delays for each antenna were determined. Residual fringe-rates were obtained by fringe-fitting a strong reference feature in the spectrum of each maser transition. At this stage in the reduction, no fringes for the 1612 MHz OH line were detected on baselines other than the shortest (Los Alamos–Pie Town) VLBA baseline. The likely cause for this non-detection is localized interstellar scattering along the line-of-sight to OH 12.8–0.9, which is relatively close to the galactic center, a direction known to exhibit anomalously high scattering on certain lines of sight (Backer 1978). Thus, the remaining discussion applies only to the H $_2$ O maser data. The fringe-rate solutions from the fringe fit were applied to all channels in the H $_2$ O maser spectrum. An iterative self-calibration and imaging procedure was then performed on the reference channel. The resulting residual phase and amplitude corrections were applied to all channels in the band.

A low-resolution cube of images  $512 \times 512$  pixels ( $\sim 500 \times 500$  mas) was formed covering the observed velocity range to locate regions of emission using a synthesized beam of  $3.0 \times 2.9$  mas. Two regions of emission were identified corresponding to spectral channel ranges from  $-37.8$  km s $^{-1}$  to  $-29.4$  km s $^{-1}$  and from  $-86.2$  km s $^{-1}$  to  $-75.7$  km s $^{-1}$ . Full-resolution cubes of images  $1024 \times 1024$  pixels ( $\sim 80 \times 80$  mas) were generated for each range of channels using a synthesized beam of  $1.98 \times 0.92$  mas. The RMS off-source noise ( $\sigma_{\text{RMS}}$ ) was typically 3 mJy beam $^{-1}$  in all channels.

In order to extract maser component parameters, two-dimensional Gaussian functions were fit to the emission in the individual channel maps. Image quality was assessed using the off-source RMS noise and the deepest negative pixel in the image. A cutoff flux density was conservatively set at  $10\sigma_{\text{RMS}}$ . Features with flux densities greater than this cutoff were fit with Gaussians to determine

component parameters. Errors in the fitted positions of identified features were computed following the methods outlined in Condon (1997). These errors ranged from  $5\mu\text{as}$  for features with high signal-to-noise, to  $60\mu\text{as}$  for features with lower signal-to-noise.

Because the emission from each maser feature extends over multiple spectral channels, it is desirable to determine a single velocity, flux density and position for each maser feature. In lieu of a full three-dimensional (3-D) Gaussian fit to the image cube, we used a flux-density-squared weighted averaging scheme to calculate nominal positions and velocities for each maser from the previously identified features. This method takes into account the increased significance of stronger emission channels. The velocities and relative offset positions thus represent weighted averages over the number of spanned channels. The assigned flux density is simply the peak value over the same range of channels.

### 3. RESULTS AND DISCUSSION

Figure 1 shows the spectral (upper sub-panels) and spatial (lower sub-panels) distributions of the  $\text{H}_2\text{O}$  masers toward OH 12.8–0.9 from the analysis of our VLBA images. Panel (a) shows the entire range of  $\text{H}_2\text{O}$  maser emission from the star. Panels (b) and (c) show enlarged views of the blue-shifted masers to the North and the red-shifted masers to the South respectively.

Focusing on the upper sub-panel of Figure 1(a), we see the previously observed spectral characteristics of the OH 12.8–0.9. The 1612 MHz OH masers form a double-peaked profile with peaks at  $-68.0$  and  $-43.7\text{ km s}^{-1}$ . The center of the profile is roughly  $-55.8\text{ km s}^{-1}$ , which is consistent with the stellar radial velocity of  $-55.5 \pm 0.5\text{ km s}^{-1}$  previously determined from the OH emission (Baud et al. 1979; Dickinson & Turner 1991). The  $\text{H}_2\text{O}$  spectrum also has a double-peaked profile, however, the  $\text{H}_2\text{O}$  masers have a greater velocity extent with peaks at  $-81.7$  and  $-33.3\text{ km s}^{-1}$ . The midpoint between these peaks ( $-57.5\text{ km s}^{-1}$ ) is slightly offset from the stellar velocity.

The lower sub-panel of Figure 1(a) shows that the masers occupy two distinct regions oriented roughly North–South on the sky with an angular separation of  $\sim 109\text{ mas}$ . The position angle of the axis of separation between the centers of the northern and southern maser regions is  $1.5^\circ$  East of North. This double-lobed distribution is consistent with VLBI observations of other water-fountain sources that show the masers occupy widely separated clumps along a presumed polar axis. Separations of  $\sim 3000\text{ mas}$  (6000 AU),  $\sim 150\text{ mas}$  (2400 AU) and  $\sim 700\text{ mas}$  (1700 AU) were determined for IRAS 16342–3814, IRAS 19134+2131 and W43A respectively (Morris et al. 2003; Imai et al. 2002, 2004) (note that the distances to all sources are somewhat uncertain, with W43A the most reliably known). The linear separation of the two maser regions toward OH 12.8–0.9 is approximately  $109\text{ AU} \times D/(1\text{ kpc})$ , where  $D$  is the distance in kpc. Unfortunately, the distance to OH 12.8–0.9 is unknown. If we assume the star is associated with the galactic center (Baud et al. 1985), at  $D \approx 8\text{ kpc}$ , then the linear separation between the blue- and red-shifted masers is  $\sim 870\text{ AU}$ .

Upon closer inspection of the blue- and red-shifted maser regions (Figure 1 (b) and (c)), we find that the masers are aligned along arc-like structures. The blue- and red-shifted arcs are approximately 10 and 12 mas (80 and 96 AU at 8 kpc) across respectively, corresponding to an opening angle for the jet that likely drives their formation of 10–13°. These arcs have an orientation that is roughly perpendicular to the separation (polar) axis. One might expect such a morphology in the case of an edge-on shock front propagating outward into a slower ambient medium. Such arc-like structures have also been observed for the H<sub>2</sub>O masers toward IRAS 16342–3814, and have been shown to have a global outward motion (Morris et al. 2003; Claussen et al. 2004). Further observations of OH 12.8–0.9 will be required to measure the proper motions of its H<sub>2</sub>O masers.

Although the radial velocity range for the H<sub>2</sub>O is not as wide as the more well-known water-fountain sources, Engels (2002) found that the shape and variations in the H<sub>2</sub>O maser spectra are consistent with this class. The velocity difference between the blue- and red-shifted H<sub>2</sub>O masers also appears to be increasing over time from early values of  $\Delta v \approx 39 \text{ km s}^{-1}$  (Engels et al. 1986) to our most recent measurement of  $\Delta v = 48.4 \text{ km s}^{-1}$ . Values of  $\Delta v$  based on the most dominant features in the H<sub>2</sub>O spectra as published in the literature are listed in Table 1 and plotted in Figure 2. All values prior to those in this work are determined from low spatial resolution (i.e. single dish and VLA) observations and are therefore subject to spatial blending of multiple maser features in a single spectral channel. From Figure 2 we see that  $\Delta v$  is obviously not constant over time, and that the masers are undergoing some form of acceleration (possibly non-linear). Since the errors in  $\Delta v$  as determined from the literature are not well known, we chose to perform a simple least-squares fit to the points assuming constant acceleration. This fit yields a value of  $2.2 \pm 0.2 \times 10^{-8} \text{ km s}^{-2}$  or  $0.68 \pm 0.06 \text{ km s}^{-1} \text{ yr}^{-1}$  for the relative acceleration of the blue- and red-shifted masers in the radial direction. The 3-D acceleration is likely larger by a factor of  $1/(\cos i)$ , where  $i$  is the inclination of the jet. The true 3-D velocities and accelerations of the masers remain to be determined through future VLBI proper motion studies.

As mentioned previously, the distance to OH 12.8–0.9 is unknown, which makes estimating the dynamical age of the outflow difficult. If we make several assumptions, namely: that the motions of the masers in the plane of the sky are comparable to the line-of-sight acceleration, that the dynamical center of the outflow is the midpoint along the axis of separation between the two maser regions, that the distance to the source is 8 kpc, and that the masers have zero initial velocity, then an upper limit to the dynamical age of the outflow can be computed. Under these assumptions, we compute a dynamical age of  $\sim 109 \text{ yr}$  using the current spatial extent of the masers and the previously determined acceleration. Similarly, a dynamical age of  $\sim 71 \text{ yr}$  is determined using the current expansion velocity of  $24.2 \text{ km s}^{-1}$  and the above acceleration. These two ages are roughly consistent with each other and with the ages computed for the three other water-fountain sources. For comparison, the dynamical ages of IRAS 16342–3814, IRAS 19134+2131 and W43A have been estimated to be  $\sim 150 \text{ yr}$  (Claussen et al. 2004),  $\sim 50 \text{ yr}$  (Imai et al. 2004) and  $\sim 40 \text{ yr}$  (Imai et al. 2002) respectively. It is interesting to note that while the small velocity spread between the blue- and red-shifted masers of OH 12.8–0.9 relative to the other water-fountain sources would

seem to indicate that the outflow is relatively young, the upper limit on the dynamical age is intermediate to those of the other sources in the class. Assuming the acceleration remains constant at  $0.68 \text{ km s}^{-1} \text{ yr}^{-1}$ , then the time to reach an outflow velocity comparable to the other water fountain sources ( $\Delta v \approx 150 \text{ km s}^{-1}$ ) is only about 220 yr or roughly twice the current dynamical age of OH 12.8–0.9.

#### 4. CONCLUSIONS

Using the VLBA we have produced the first high-resolution interferometric images of the  $\text{H}_2\text{O}$  masers toward the OH/IR star OH 12.8–0.9. These images show that the masers lie in a double-lobed structure typical of objects belonging to the water-fountain class of sources. We also find that the two groupings of masers are arranged in arc-like structures suggestive of a bow-shock morphology. The spatio-kinematic structure determined from our VLBA observations provides strong evidence that OH 12.8–0.9 is indeed a water fountain source, and that the outflow is accelerating in the line-of-sight direction.

In future observations, we hope to map the scatter-broadened OH masers using a shorter-baseline connected element interferometer such as the VLA or the Multi-Element Radio Linked Interferometer (MERLIN). Such observations should verify that the  $\text{H}_2\text{O}$  masers lie further from the underlying star than the OH masers; a characteristic evident in the other water-fountain sources. We also plan to undertake a multi-epoch VLBI campaign to study the proper motions of the  $\text{H}_2\text{O}$  masers. Such observations should allow us to characterize the three-dimensional motion of the masers, determine the distance to OH 12.8–0.9, and determine a dynamical center and age for the outflow.

KBM wishes to thank the NRAO for supporting him during a short research leave from his day job in Washington, DC and TEK for her continued support.

## REFERENCES

- Baud, B., Habing, H. J., Matthews, H. E. & Winnberg, A. 1979, *A&AS*, 36, 193
- Baud, B., Sargent, A. J., Werner, M. W. & Bentley, A. F. 1985, *ApJ*, 292, 628
- Backer, D. C. 1978, *ApJ*, 222, L9
- Claussen, M., Sahai, R., & Morris, M. 2004, *Astronomical Society of the Pacific Conference Series*, 313, 331
- Condon, J.J. 1997, *PASP*, 109, 166
- Dickinson, D. F. & Turner, B. E. 1991, *ApJS*, 75, 1323
- Engels, D. 2002, *A&A*, 388, 252
- Engels, D. & Lewis, B. M., 1996, *A&AS*116, 117
- Engels, D., Schmid-Burgk, J. & Walmsley, C. M. 1986, *A&A*, 167, 129
- Gómez, Y., Rodríguez, L. F., Contreras, M. E. & Moran, J. M. 1994, *Rev. Mex. Astron. Astroph.*, 28, 97
- Imai, H., Morris, M., Sahai, R. Hachisuka, K. & Azzolini F, J. R. 2004, *A&A*, 420, 265
- Imai, H., Obara, K., Diamond, P. J., Omodaka, T. & Sasao, T. 2002, *Nature*, 417, 829
- Likkell, L., Morris, M., Maddalena, R. J. 1992, *A&A*, 256, 581
- Likkell, L. & Morris, M. 1988, *ApJ*, 329, 914
- Morris, M. R., Sahai, R. & Claussen, M. 2003, *RevMexAA*, 15, 20
- Sahai, R., te Lintel Hekkert, P., Morris, M. 1999, *ApJ*, 514, L115
- te Lintel Hekkert, P., Versteeg-Hensel, H. A., Habing, H. J. & Wiertz, M. 1989, *A&AS*, 78, 399
- Tylenda et al. 2003, *A&A*, 405, 627



Table 1. Velocity separation of dominant water maser components.

Obs. Date (yr)	$\Delta v$ ( $\text{km s}^{-1}$ )	Spectral res. ( $\text{km s}^{-1}$ )	Notes Reference, features used
1985.30	34.7	0.2	(1), strongest features - matched to hi-res ep.
1985.58	36.1	0.2	(1), strongest features - matched to hi-res ep.
1987.45	38.4	0.16	(2), feature F - feature N
1988.51	38.9	0.16	(2), feature F - feature N
1992.47	42.3	2.6	(3), (blend of blue and red features)
1995.19	44.5	0.16	(2), feature B - feature O
1999.09	45.5	0.16	(2), feature B - feature O
2004.57	48.4	0.2	(4), strongest features

Note. — References: (1) Engels et al. (1986), (2) Engels (2002), (3) Gómez et al. (1994), (4) this work.

Figure Captions

Fig. 1.— The H<sub>2</sub>O maser emission toward OH 12.8–0.9. In panels (a), (b) and (c), the top sub-panels show the spectra formed by plotting maser component flux density versus LSR velocity, color-coded according to maser velocity. A dark solid line in each upper sub-panel represents the scalar-averaged cross-power spectrum on the Los Alamos–Pie Town VLBA baseline. A dashed line in the top sub-panel of (a) represents the scalar-averaged cross-power spectrum of the OH masers (with the flux density scaled by a factor of 0.5) from the Los Alamos–Pie Town baseline. The lower sub-panels in (a), (b) and (c) plot the spatial distribution of the H<sub>2</sub>O masers with point-color representing the corresponding velocity bin in the spectrum and point-size proportional to the logarithm of the maser flux density. Panel (a) shows all H<sub>2</sub>O maser components from our VLBA observations. A dashed line represents the axis of separation between the centers of the blue- and red-shifted masers at a position angle of 1.5° East of North. The “×” symbol represents the midpoint of the bipolar distribution. Panels (b) and (c) show expanded views of the blue- and red-shifted maser features respectively. Errors in the positions of the features are smaller than the data points for all panels.

Fig. 2.— Plot showing the measured velocity separation ( $\Delta v$ ) of the dominant water maser features as a function of time from values listed in Table 1. The line represents a linear least-squares fit to the data and indicates a constant acceleration of  $0.68 \text{ km s}^{-1} \text{ yr}^{-1}$ .

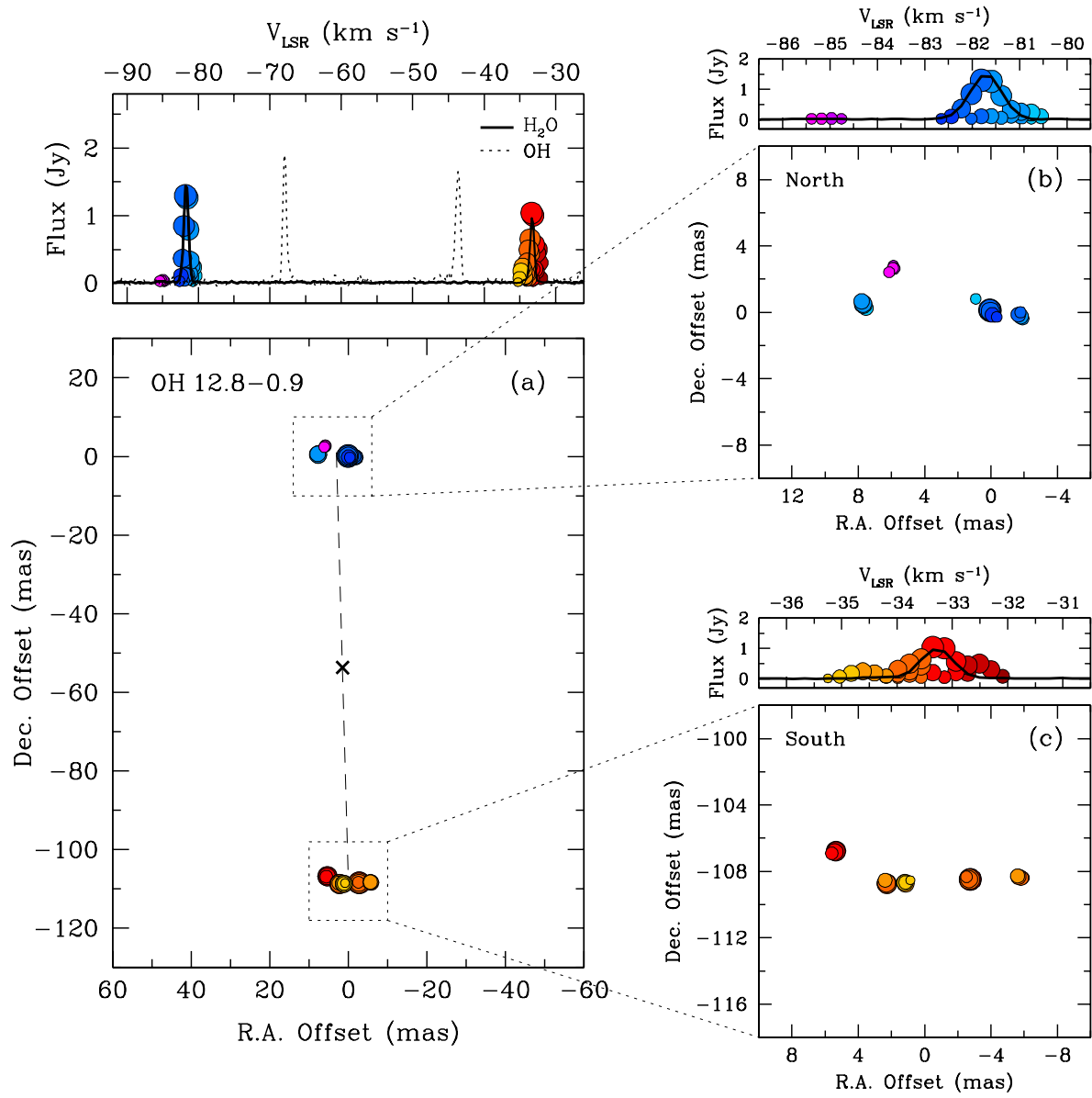


Figure 1

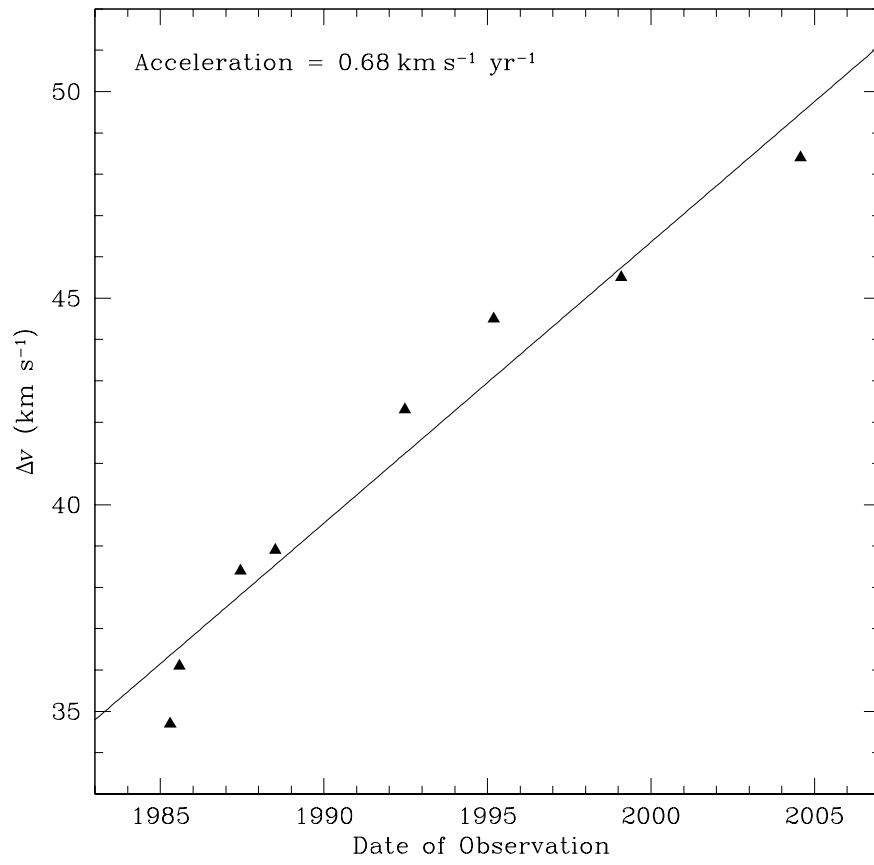


Figure 2